Predicting Daily Mean Wind Speed in Europe Weeks ahead from MJO Status

LLORENÇ LLEDÓ

Barcelona Supercomputing Center, Barcelona, Spain

FRANCISCO J. DOBLAS-REYES

Barcelona Supercomputing Center and ICREA, Barcelona, Spain

ABSTRACT

The Madden–Julian oscillation (MJO), a prominent feature of the tropical atmospheric circulation at subseasonal time scales, is known to modulate atmospheric variability in the Euro-Atlantic region. However, current subseasonal prediction systems fail to accurately reproduce the physical processes involved in these teleconnection mechanisms. This paper explores the observed impact of strong MJO events on surface wind speed over Europe. It is found that some MJO phases are accompanied by strong wind anomalies in Europe. After showing that this teleconnective mechanism is not present in the predictions of the ECMWF monthly forecasting system, a methodology to reconstruct forecasts of daily mean wind speed in the continent weeks ahead is proposed. This method combines MJO forecasts from the S2S project database and the observed teleconnection impacts in the historical records. Although it is found that strong MJO events cannot be skillfully predicted more than 10 days ahead with current prediction systems, a theoretical experiment shows that this method can effectively transform a dynamical MJO forecast into a probabilistic wind speed prediction in Europe.

1. Introduction

The Madden–Julian oscillation (MJO) is the dominant mode of atmospheric variability at subseasonal time scales in the tropics. It consists of an enhanced convection cell traveling west to east along the equator, completing a whole lap of Earth in 30–60 days (Madden and Julian 1971, 1972; Zhang 2005). Several studies have shown that the MJO modulates many atmospheric phenomena at the intraseasonal time scales (see Zhang 2013 for a review). Extratropical circulation is specially affected through excitation of tropospheric Rossby waves but also through the stratosphere (Barnes et al. 2019). For instance Lin et al. (2009) and Cassou (2008) established a connection between the MJO and the

North Atlantic Oscillation (NAO), which is the first mode of atmospheric variability over the Euro-Atlantic region. This relationship depends on the location of the enhanced convective activity (i.e., the MJO phase), but also on its intensity, propagation speed, or lifetime (Zheng and Chang 2019).

A good description of the physical processes that play a role in MJO propagation (viz., convection, moisture advections and underlying sea surface temperatures) is key to forecast the MJO evolution (Kim et al. 2019), while an adequate representation of the teleconnective mechanisms that derive from it (diabatic heating due to convection and propagation of Rossby waves through background flow) would in turn allow to anticipate its impact on the extratropics (Zheng and Chang 2019). The S2S project (Vitart et al. 2017) brings together subseasonal predictions from several operational centers and allows a systematic study of the MJO prediction skill in these systems (Vitart 2017; Lim et al. 2018), which show that the ECMWF model has a clear lead in predicting the MJO evolution. This system has a skillful prediction horizon of 36 days [defined as the day at which bivariate correlation (Lin et al. 2008) goes below 0.5]. However, Vitart (2017) also shows that all models

---

in the S2S database fail to reproduce the teleconnection impacts in the Northern Hemisphere. Specifically, geopotential height anomalies 11 to 15 days after the MJO was in phase 3 or 7 are too weak in the models when compared to observations (Figs. 7 and 8 in Vitart 2017). Summarizing, the ECMWF model does a decent job in simulating MJO propagation, but fails to reproduce the teleconnective impacts over Europe, and this is a generalized behavior of subseasonal prediction systems.

This scenario opens the door to employ hybrid dynamical-statistical approaches (i.e., combine a dynamical forecast of the MJO state with the observed teleconnection impacts) to produce forecasts for specific sectoral applications. One socioeconomic sector that can benefit from this approach is the wind energy sector. While power producing companies, traders and grid operators use weather forecasts up to 10 days ahead routinely for its daily operations, forecasts of daily mean wind speed weeks ahead could be useful for many of them (Soret et al. 2019).

A methodology that combines a probabilistic seasonal forecast of ENSO with its past observed wind speed impacts has been proposed in Torralba (2019) and applied with success in some regions where dynamical models fail to reproduce ENSO teleconnections. However, the MJO is a traveling wave and its state has to be described with two indices: either the two components of an empirical orthogonal function (EOF) decomposition (usually known as RMM1 and RMM2; Wheeler and Hendon 2004), or a phase and an amplitude index. Therefore this method, which was devised for one single index, cannot be directly employed here, and new algorithms need to be designed.

In this work the impact of strong MJO events on wind speeds over Europe is analyzed through reanalysis stratifications as a function of the MJO phase. Then the same stratifications are performed for the ECMWF subseasonal predictions to confirm that the teleconnections are not well reproduced for wind speed. After that, a novel method to combine past observed teleconnection effects with an MJO forecast is described and analyzed.

2. Datasets and methods

a. Datasets

1) SURFACE WIND OBSERVATIONS

Observational estimates of surface winds (i.e., at 10 m) for the period 1981–2017 have been obtained from the fifth generation of the European Centre for Medium-Range Weather Forecasts (ECMWF) reanalysis (ERA5)

[Copernicus Climate Change Service (C3S) 2017]. Some findings have also been confirmed with winds at 100 m above ground from ERA5 and at 50 m from NASA's Modern-Era Retrospective Analysis for Research and Applications-2 (MERRA2, Gelaro et al. 2017). Daily mean speeds have been computed from hourly values in both datasets. Those two reanalyses provide the best global estimates of observed surface or near-surface wind according to a comparison of several global reanalysis datasets (Ramon et al. 2019). ERA5 has been obtained on a Gaussian F320 grid (a resolution of $0.281\,25°$ or $\sim 28\,km$) while MERRA2 has a regular grid with a resolution of $0.625° \times 0.5°$.

2) SURFACE WIND PREDICTIONS

Subseasonal predictions of surface wind from the ECMWF monthly forecasting system (MFS) (ECMWF 2019; Vitart 2004) have been employed to evaluate the strength of the MJO teleconnection response and estimate future wind speed. Daily mean winds have been computed from 6-hourly outputs for all the available forecast times up to 46 days ahead and for the 11 ensemble members. The full hindcasts associated with the 2018 real-time forecasts—covering the 1998–2017 period—have been employed to obtain a consistent and long record of retrospective predictions. The data, which corresponds to IFS cycle CY43R3, have been obtained from ECMWF MARS on a regular Gaussian F320 grid ($\sim 28\,km$ of horizontal resolution, which is the same resolution of ERA5).

3) MJO OBSERVATIONS

The MJO is a propagating wave, and many methods have been proposed in the literature to describe its state. Generally speaking, two coordinates that specify its phase and amplitude are required. Here, observed MJO daily indices have been retrieved from two separate sources, both using a combined (or multivariate) EOF decomposition. First, the Real-Time Multivariate MJO indices (RMM) described in Wheeler and Hendon (2004) have been obtained from Australian Bureau of Meteorology (BoM) (http://www.bom.gov.au/climate/mjo/graphics/rmm.74toRealtime.txt). These RMM components are computed operationally from satellite outgoing longwave radiation (OLR, a proxy for convective activity) and NCEP–NCAR reanalysis (Kalnay et al. 1996) zonal winds at 850 and 200 hPa, after removing ENSO-related variability and the mean of the 120 most recent days. Second, daily indices derived fully from ERA-Interim fields (Dee et al. 2011) have been retrieved from the S2S database (Vitart 2017) in a methodology that differs slightly from the Wheeler and Hendon (2004) method (ENSO-related variability is not

removed; see Gottschalck et al. 2010 for details). While the BoM index has been widely used to monitor the MJO and evaluate its teleconnective impacts, the S2S index was adopted by the S2S project to develop and verify forecasts. The MJO phase and amplitude have been derived from RMM components in both datasets.

4) MJO PREDICTIONS

MJO retrospective predictions from the ECMWF MFS-2018 hindcasts—covering the 1998–2017 period—have been retrieved from the S2S database (Vitart et al. 2017). The MJO predictions employ the method described in Vitart (2017) and are methodologically consistent with the S2S ERA-Interim-derived MJO observations. MJO S2S forecasts have been obtained individually for each ensemble member and for the ensemble mean (i.e., computed from ensemble-mean fields). MFS has been selected among all models within the S2S database because, as explained above, it has been shown to be the best model in forecasting the MJO evolution (Vitart 2017).

b. Methods

1) STRATIFICATIONS

Wind speed conditions in Europe during strong MJO events are analyzed through stratifications of daily mean wind speed. Stratifications—also known as composite maps—consist of separate statistical analyses of a sample that is partitioned into subgroups by an external factor. In this case the sample of observed 1981–2017 daily mean wind speeds is partitioned into nine groups by the observed MJO phase and amplitude, producing a disjoint and exhaustive partition: the distribution of wind speed values is analyzed separately for those days when the MJO is in one of its eight phases with a strong amplitude (amplitude > 2; see Fig. S6 in the online supplemental material for a graphical representation of those nine groups and a short digression on the threshold selected to define strong MJO events). For each of these groups, the mean wind speed anomalies with respect to the whole sample have been computed at each grid point and expressed as a percentage. This normalization allows to plot anomalies over land and ocean (where winds and absolute anomalies are much higher) in the same scale. It also allows a fair comparison between wind speed anomalies at different heights above ground (see Figs. S1, S2), for the same reasons.

As the MJO activity tends to be stronger from October to March, the analysis focuses on this period of the year. The extratropical impact of the MJO depends on the location and strength of the tropical convection (i.e., MJO phase and amplitude), but also on the mean zonal flow in the extratropics, which modulates the propagation of Rossby waves. To account for differences in mean flow during this extended winter period, the stratifications have been produced separately for October to December (OND) and January to March (JFM). Separate stratifications for each month would have resulted in too small samples. Notice that daily anomalies have been computed with respect to OND and JFM averages instead of using a smoothed daily climatology. The impact of this simplification is small because intraseasonal variability of daily winds is much higher than the variation in climatological mean wind speed during this 3-month period. Lagged stratifications (i.e., a number of days after strong MJO events occurred) have also been studied to account for Rossby wave propagation time. The statistical significance of the stratifications has been assessed with a two-tailed Student's t test with a confidence level of 95%.

First, 1981–2017 winds from ERA5 and MERRA2 have been stratified. The sensitivity to the analyzed period has been assessed comparing the whole period (1981–2017) to a shorter period (1998–2017). The impact of the MJO index definition (i.e., BoM or S2S index) has also been considered.

Then, wind speeds from the MFS have been stratified similarly, according to the forecasted (S2S) MJO index at several lead times. The S2S MJO indices are available separately for each of the 11 ensemble members of MFS hindcasts. Only the members that predict a strong MJO event are included in the stratification. Results have been grouped for forecast days 1 to 4, 5 to 11 (week 1), 12 to 18 (week 2), and so on, following the convention in Vitart (2004). In this case the anomalies have been computed with respect to a lead-time-dependent climatology (i.e., separately for each of the forecast weeks considered). As the forecasts have an ensemble available, the sample sizes for the MFS stratification are larger than for the observational stratification, impacting the statistical significance (i.e., weaker impacts are detected as significant).

2) MOST FREQUENT TERCILE MAPS

The mean value of a sample (employed in the stratifications) is not a very meaningful statistic and overly simplifies the sample distribution properties. For instance we can have many wind speed distributions with the same mean but differing variability. To overcome this limitation, observed tercile frequencies (frequency of above-normal, normal, and below-normal wind conditions) during strong MJO events complement the mean wind stratifications. Maps of the most frequently observed tercile display the occurrence frequency of the

tercile category that has occurred more times during each strong MJO phase. To construct these maps, first the 33rd and 66th percentiles of the 1981–2017 wind speed distribution are obtained for each grid point (separately for each month). Then the number of observations that are above, below, and within these thresholds is counted for all days in each strong MJO phase. This procedure has previously been used to present probabilistic climate predictions from large ensembles in a simplified way and overcome the dangers of using ensemble-mean anomalies (Jupp et al. 2012; Torralba et al. 2016).

3) HYBRID DYNAMICAL–STATISTICAL SURFACE WIND PREDICTIONS

Under the hypothesis that MJO prediction is accurate at subseasonal time scales, but that the representation of teleconnection mechanisms is weak or defective in dynamical models, a hybrid dynamical–statistical method is proposed here. The method combines dynamical MJO forecasts with past observed relationships to reproduce the impact forecasts (wind speeds in this case) in a perfect prognosis approach. The aim is to produce a simple probabilistic forecast of daily mean wind speed in the form of tercile probabilities, mimicking typical subseasonal probabilistic products derived from ensemble prediction systems. The method uses observed tercile frequencies conditioned on the observation of an MJO phase [as in section 2b(2)] as forecast probabilities. If the forecasted MJO amplitude ($\widehat{\text{MJO}}_{\text{ampl}}$) is less than 2, then 1/3 of probability is assigned to each category. Otherwise when a strong MJO is anticipated, past observed frequencies for each tercile during the forecasted MJO phase ($\widehat{\text{MJO}}_{\text{ph}}$) are used as forecast. We call this method conditional climatology. For each day d it is computed as

$$\text{clim}|_{\text{MJO}}(d) = \begin{cases} \text{clim}(x) & \text{if} \quad \widehat{\text{MJO}}_{\text{ampl}}(d) < 2 \\ \text{clim}(x|\text{MJO}_{\text{ph}}(x) = 1 \quad \text{and} \quad \text{MJO}_{\text{ampl}}(x) \geq 2) & \text{if} \quad \widehat{\text{MJO}}_{\text{ph}}(d) = 1 \quad \text{and} \quad \widehat{\text{MJO}}_{\text{ampl}}(d) \geq 2 \\ \vdots \\ \text{clim}(x|\text{MJO}_{\text{ph}}(x) = 8 \quad \text{and} \quad \text{MJO}_{\text{ampl}}(x) \geq 2) & \text{if} \quad \widehat{\text{MJO}}_{\text{ph}}(d) = 8 \quad \text{and} \quad \widehat{\text{MJO}}_{\text{ampl}}(d) \geq 2 \end{cases}, \quad (1)$$

where x are all days in the historical observational record and a hat represents a forecasted value. In the equation above, "clim" can be any climatology statistic, such as the mean (deterministic forecast), or tercile probabilities (probabilistic forecast), as employed here.

4) VERIFICATION OF PROBABILISTIC FORECASTS

The forecasts of tercile probabilities that are produced with the conditional climatology method have been verified employing the ranked probability skill score (RPSS) (Jolliffe and Stephenson 2012), which is specifically designed for ordered multicategorical probabilistic forecasts. For each day, the observed tercile category is determined from ERA5 and used as verification truth. The RPSS compares the scores for the conditional climatology forecasts to the scores of a climatology (i.e., 33% of probability for each tercile category independently of the MJO status), and gives the relative improvement over this baseline: positive RPSS values denote better performance than climatology, with the value of one corresponding to a perfect forecast.

When using statistical models, and to obtain fair results, it is important that the verification is made with an independent sample that has not been employed during the model construction. The leave-one-out cross-validation technique (Wilks 2011) consists in repeating the training and verification steps multiple times by setting aside one observation each time that is not used for building the model and is reserved for verification only. This allows us to estimate the model parameters with all but one observations, and is suitable for small sample sizes. Specifically for the conditional climatology method, this means that the observed category for a given day is not included in the computation of the observed tercile frequencies used as forecast for that day.

3. Results

a. Observed teleconnection impacts

To characterize wind speed anomalies over Europe during strong MJO events, the daily mean ERA5 surface wind speeds have been stratified employing MJO time series [see section 2b(1) for details]. Figure 1 shows the JFM composite maps for both BoM and S2S observed MJO indices and for two different periods, 1981–2017 and 1998–2017. For the long period and the BoM index (first column) the 733 strong MJO events recorded in JFM are related to systematic anomalies over the North Atlantic ocean and Europe (around 10% to 15%, but up to ±40% in some cases), although those anomalies are located in different areas for each of the phases.
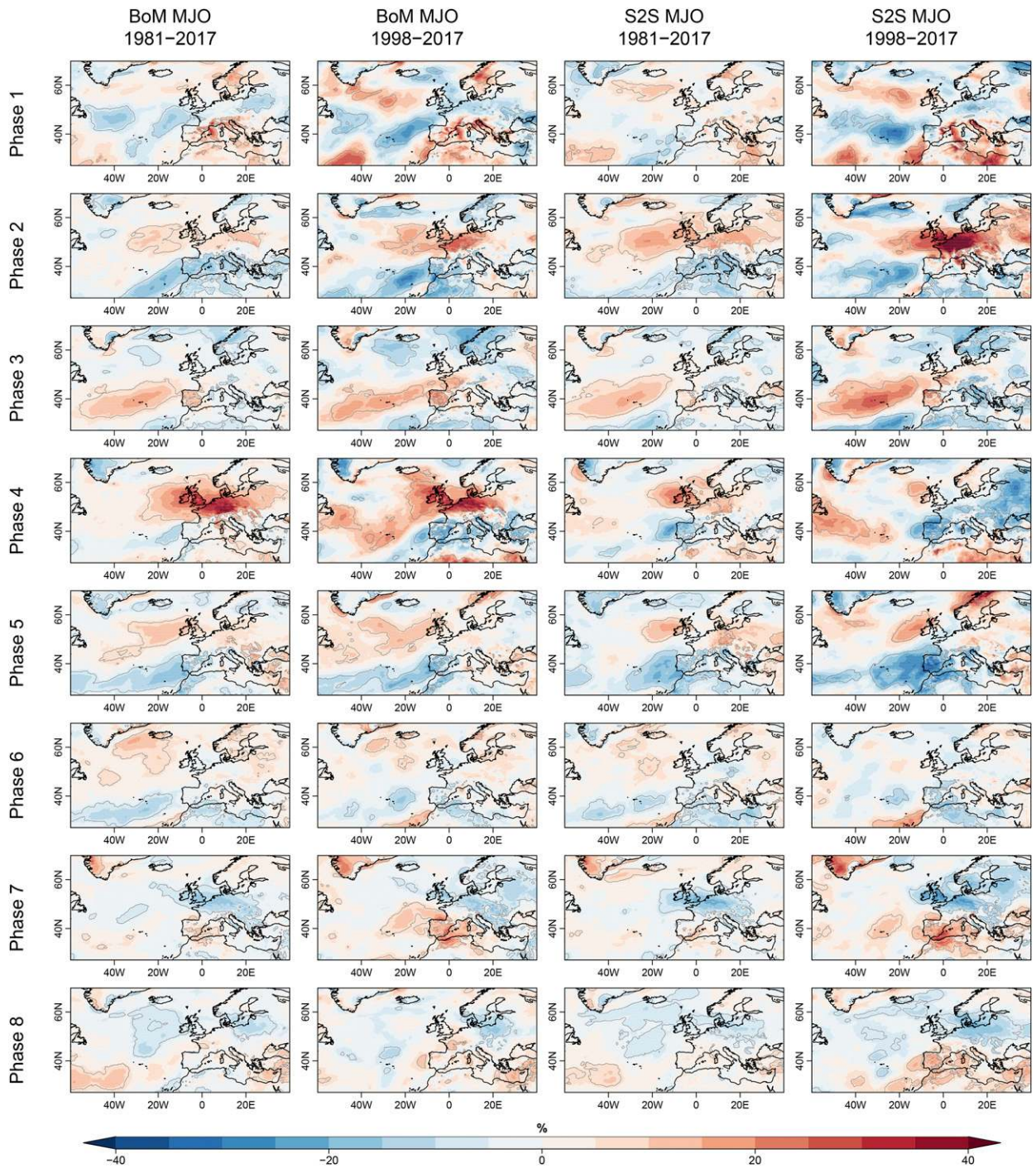
FIG. 1. JFM surface wind anomalies in Europe during strong MJO events (amplitude > 2) for each MJO phase (rows), expressed as a percentage of mean wind speed in the period. Columns show results for different periods and MJO indices: (first column),(second column) BoM MJO index and (third column),(fourth columns) S2S MJO index computed from ERA-Interim. Note that the first and third columns use a long period (1981–2017), while the second and fourth columns use a shorter period (1998–2017). Gray contours indicate statistical significance at the 95% level.
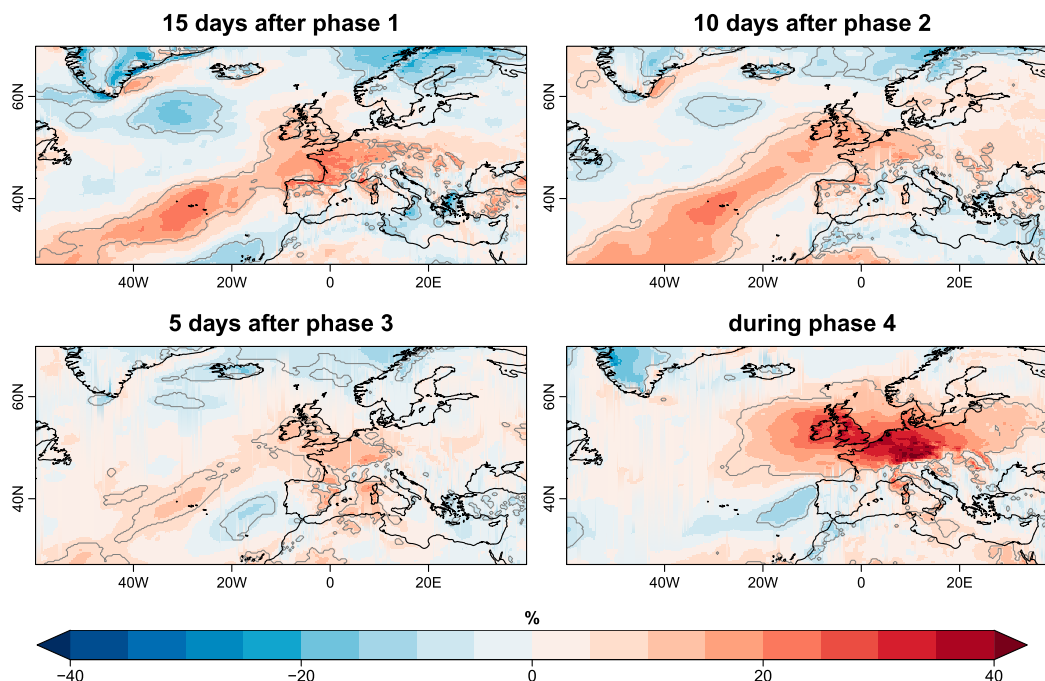
FIG. 2. JFM surface wind anomalies in Europe (top left) 15, (top right) 10, (bottom left) 5, and (bottom right) 0 days after strong MJO events (amplitude > 2) in phases 1, 2, 3, and 4, respectively, expressed as a percentage of mean wind speed in the 1981–2017 period and for the BoM MJO index. Gray contours indicate statistical significance at the 95% level.

In particular, during phase 4 (78 events), winds are 30% to 40% higher than average over the British Isles and central Europe, while during phase 7 (132 events) this region experiences weaker winds than average. Phase 1 also shows a strong signal over the western Mediterranean, with daily mean winds around 30% above average in some spots. The whole Iberian Peninsula is also affected by phases 2, 3, and 5. A similar analysis for 50- and 100-m winds—the heights at which wind turbines are typically installed— reveals the same anomaly patterns (see Figs. S1, S2). The number of strong events in each phase, and associated sea level pressure anomalies can also be seen in Figs. S1 and S2.

These results for BoM MJO index stratifications are in line with existing literature that shows that the atmospheric circulation in the Euro-Atlantic region in boreal winter is conditioned on the MJO (Lin et al. 2009; Cassou 2008). Indeed, the wind anomalies in the first column of Fig. 1 and the associated pressure patterns in Fig. S1 resemble various circulation patterns: phases 7 and 8 recall a negative NAO pattern or a Scandinavian blocking, while phases 2 to 5 bear a resemblance to positive NAO or east Atlantic patterns. Lin et al. (2009) and Cassou (2008) show that the NAO response to the MJO forcing is delayed between 5 and 15 days. The time scale of this teleconnection depends on "differing

lengths of the teleconnection pathway for different MJO phases, differing propagation speeds of MJO events yielding differing teleconnection responses, and the NAE region simultaneously responding to multiple positions of MJO convection considering different lags" (Lee et al. 2019). However, lagged wind speed stratifications 5 to 15 days after strong MJO events produced weaker impacts. For instance, Fig. 2 shows lagged stratifications 15, 10, 5, and 0 days after phases 1, 2, 3, and 4, respectively. The anomalies seen during phase 4 are stronger than those seen the days after phases 1 to 3. On average, it takes around 5 days for the MJO to propagate from one phase to the next one. However, 15 days after a phase 1 strong MJO event only a small portion of days have a phase 4 strong MJO (see Fig. S7), and similarly, of all the days with a phase 4 strong MJO event only a few of them were in a phase 1 strong MJO 15 days before. This diversity of MJO events—differing MJO propagation but differing Rossby wave propagation as well (Wang et al. 2019; Zheng and Chang 2019)—difficult isolating the effects of the different lagged responses to the MJO phases.

Additionally, Fig. S3 provides a detailed analysis day by day of the lagged impacts of MJO phases for a single location near Frankfurt (a representative spot of NAO impact on wind). It can be seen how wind anomalies in

that location precede the initiation of MJO events in phase 1. This is also consistent with some research that found that the NAO can influence tropical winds in the Atlantic and African areas after some lag and initiate or amplify MJO events during phases 8 and 1 (Barnes et al. 2019; Lin et al. 2009). Indeed tropical winds have an active role in the MJO RMM computation, and sometimes large-scale circulation anomalies precede MJO convection (Liu et al. 2016; Straub 2013). Under all these circumstances, it is important to note that the stratification results presented cannot distinguish causality links between MJO activity and extratropical wind speed anomalies. Despite not knowing the exact reasons behind the strong wind anomalies that accompany strong phase 4 MJO events, that information can still be useful for statistical modeling (section 3f).

b. Sensitivity to period and index definition

Although the BoM index is typically used in the majority of works that study observed MJO teleconnections and impacts (e.g., Cassou 2008; Lin et al. 2009; Zhang 2013), most of the work focusing on MJO forecasting (and in particular the S2S project) employs a computation variant described in Gottschalck et al. (2010). As the present work combines both of the worlds, the observed impact has also been assessed employing the S2S ERA-Interim-derived index for the 1981–2017 period (third column in Fig. 1). Wind speed from these stratifications bears some resemblance to the results obtained with the BoM stratifications (first column). However, in general the values are smaller and the patterns have important differences at the regional scale. An analysis of the days that are classified as strong MJO events by each of the two indices has been performed (see Fig. S4), and although the bivariate correlation (Lin et al. 2008; Rashid et al. 2010) between both MJO indices is 0.90, and its amplitudes have a Pearson correlation of 0.81, the days included in each strong MJO phase category are very different for both indices, resulting in the discrepancies aforementioned.

Figure 1 also presents the stratifications for a shorter period (that will be used later in section 3d for the MFS hindcasts). We find that the results are also sensitive to the sample period, and reducing the number of years (differences between first and second columns, or between the third and fourth columns) produces some differences in pattern position and magnitude (e.g., see phase 2 in central Europe or phase 4 in the Iberian Peninsula). Conversely, the results are not sensitive to the observational wind speed dataset employed, and stratifications made with MERRA2 show almost identical results (Figs. S1, S2). These results are useful for the interpretation of the quality

of the prediction-based wind speed stratification results in section 3d.

c. Distribution of wind speed values under strong MJO events

The stratifications presented so far show the mean wind speed anomalies associated with strong MJO events but do not inform about the full distribution of observed values during each MJO phase. To exemplify this, the whole distribution of daily mean wind speed values associated with each strong MJO phase (according to BoM index) is shown in Fig. 3 for a grid point over Frankfurt (49.88°N, 8.44°E). The selected location is a spot of high correlation between the NAO and surface wind, and therefore it is a good representative of the interactions between the NAO and the MJO. To better understand how those distributions differ from the whole-period climatology, the 10th, 33rd, 66th, and 90th percentiles of the climatology (referred as P10, P33, P66, and P90, respectively) have been used to color the distributions and compute tercile occurrence frequencies. For instance, for phase 4 most of the daily wind speed values (61%) fall above P66, with a 31% of values above P90. But for phase 1, the normal category (between P33 and P66) is the most frequent category indicating that either high or low wind speeds are less frequent under this MJO phase. This figure also shows that although the MJO can influence the wind speed over Europe, the teleconnective mechanism is not straightforward, and other elements can interact with it and determine the final wind speed values [such as the phase of the quasi-biennial oscillation (Lim et al. 2019; Zhang and Zhang 2018), the strength of the stratospheric polar vortex (Barnes et al. 2019), the ENSO phase (Lee et al. 2019), or the intensity and location of the westerly subtropical jet that guides Rossby wave propagation (Adames and Wallace 2014)].

To summarize part of the information presented in Fig. 3 in a map but still include more information on the distribution that just its mean value, the most frequent tercile maps of the wind speed have been produced for each MJO phase (see Fig. 4). The maps present the observed frequency of the most frequent tercile at each point and for each MJO phase [see section 2b(2)]. Those plots are more informative than the mean anomaly. The plots have been produced for the whole globe to highlight the connections between tropical winds (which are employed in the computation of MJO) and wind anomalies over the extratropics. Phases 4 and 5 tend to be associated with above normal-wind speed conditions in the tropics while during phases 8 and 1 the tropics are more likely to experience weak (below-normal) winds. The patterns that were described in Fig. 1 for Europe
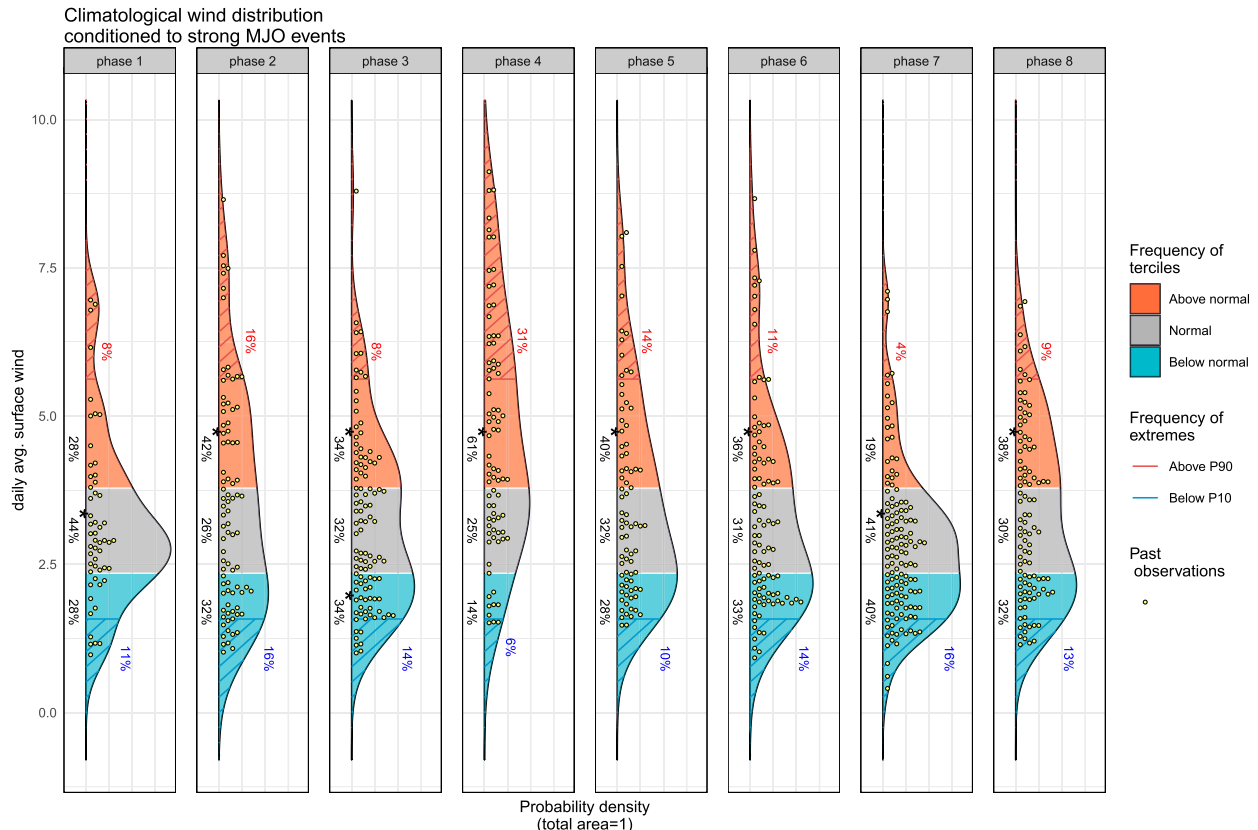
FIG. 3. Observed (ERA5, 1981–2017) daily mean wind speed distribution near Frankfurt (49.88°N, 8.44°E) for each of the eight MJO phases when amplitude is higher than 2 according to BoM index. Frequencies of occurrence of the tercile categories below-normal, normal, and above-normal conditions have been colored in red, gray, and blue, respectively, and annotated, while red (blue) stripes indicate frequency of exceeding (not reaching) the 90th percentile (10th percentile). Yellow dots indicate individual daily observations. A star indicates the most frequent tercile category.

can be seen here as well, with a high frequency of above-normal conditions during phase 4 over central Europe, or a high frequency of below-normal conditions over the Iberian Peninsula during phase 2. Important connections can be seen as well in North America and other extratropical regions, although those have not been explored further in this paper.

d. Teleconnection impacts in the subseasonal simulations

To understand the ability of ECMWF subseasonal forecasts to reproduce the observed MJO impacts over Europe, the stratifications have been applied also to the MFS forecasts at different forecast times, employing the MFS MJO forecasts from S2S. Figure 5 compares the results for forecast days 1 to 4, 5 to 11 (week 1), and 12 to 18 (week 2) with reanalysis (ERA5) winds stratified with the S2S MJO ERA-Interim index. The results are shown for phases 2, 5, and 7 only, which are the phases with stronger impacts over Europe for the S2S MJO index

(see last column of Fig. 1). The impacts for the first 4 days of forecasts resemble the observed patterns, although amplitudes are weaker. With longer forecast times (weeks 1 and 2) the impacts become even weaker, that is, for those days where the model predicts a strong MJO event 1 or 2 weeks ahead, the associated wind speed predictions over Europe do not reproduce the expected teleconnection effects beyond week 2. Those results are in agreement with Vitart's (2017) Figs. 7 and 8. From this we conclude that MFS is not able to reproduce the MJO teleconnection impacts over European wind speeds more than a couple of weeks ahead.

e. Verification of subseasonal forecasts of strong MJO events

In view of the limited ability of the ECMWF subseasonal predictions to reproduce the expected wind speed impacts of MJO over Europe, the conditional climatology method described in section 2b(3) can be used to combine dynamic MJO forecasts with its
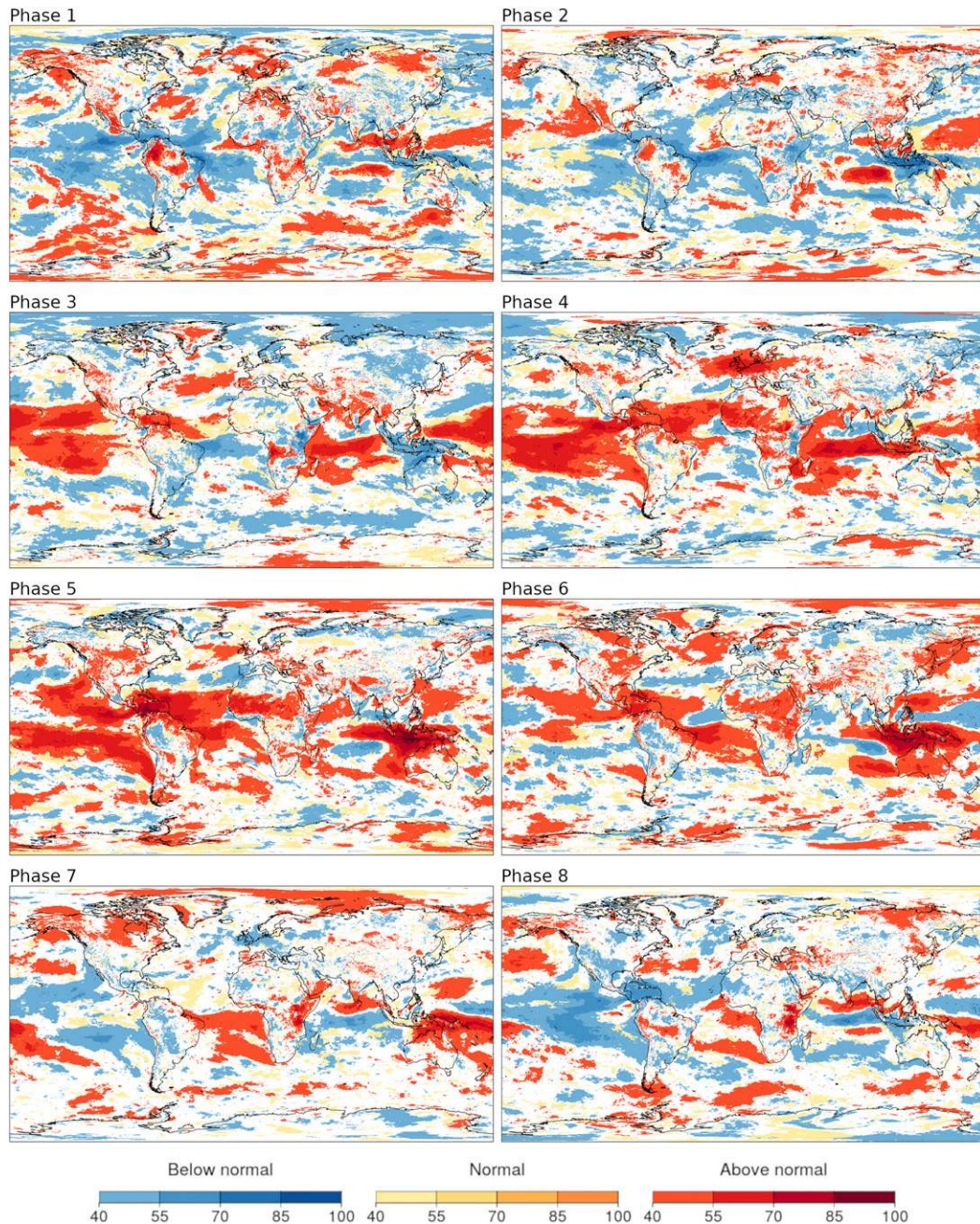
FIG. 4. Global maps of most frequently observed tercile during strong MJO events for each of its phases. The distribution of daily mean wind speed values from ERA5 in JFM 1981–2017 is analyzed according to the BoM MJO index. At each grid point and for each MJO phase, individual values of the distribution are grouped in three tercile categories (above-normal, normal, and below-normal wind speed conditions) and the frequency of each category is computed. The color indicates the most frequently observed tercile category, while color intensity indicates its associated frequency of occurrence.

observed wind speed impacts. As a first step, the quality of the MJO forecasts needs to be assessed. Many studies of MJO forecast verification employ the forecast time at which bivariate correlation goes below 0.5 (Lin et al. 2008; Lim et al. 2018; Vitart 2017) as a threshold of a

skillful prediction, and for MFS they show skill up to 36 days ahead. But in order to employ MJO forecasts from the S2S database with the conditional climatology method, we need to understand how accurate the forecasts are for each of the strong MJO phases. That could
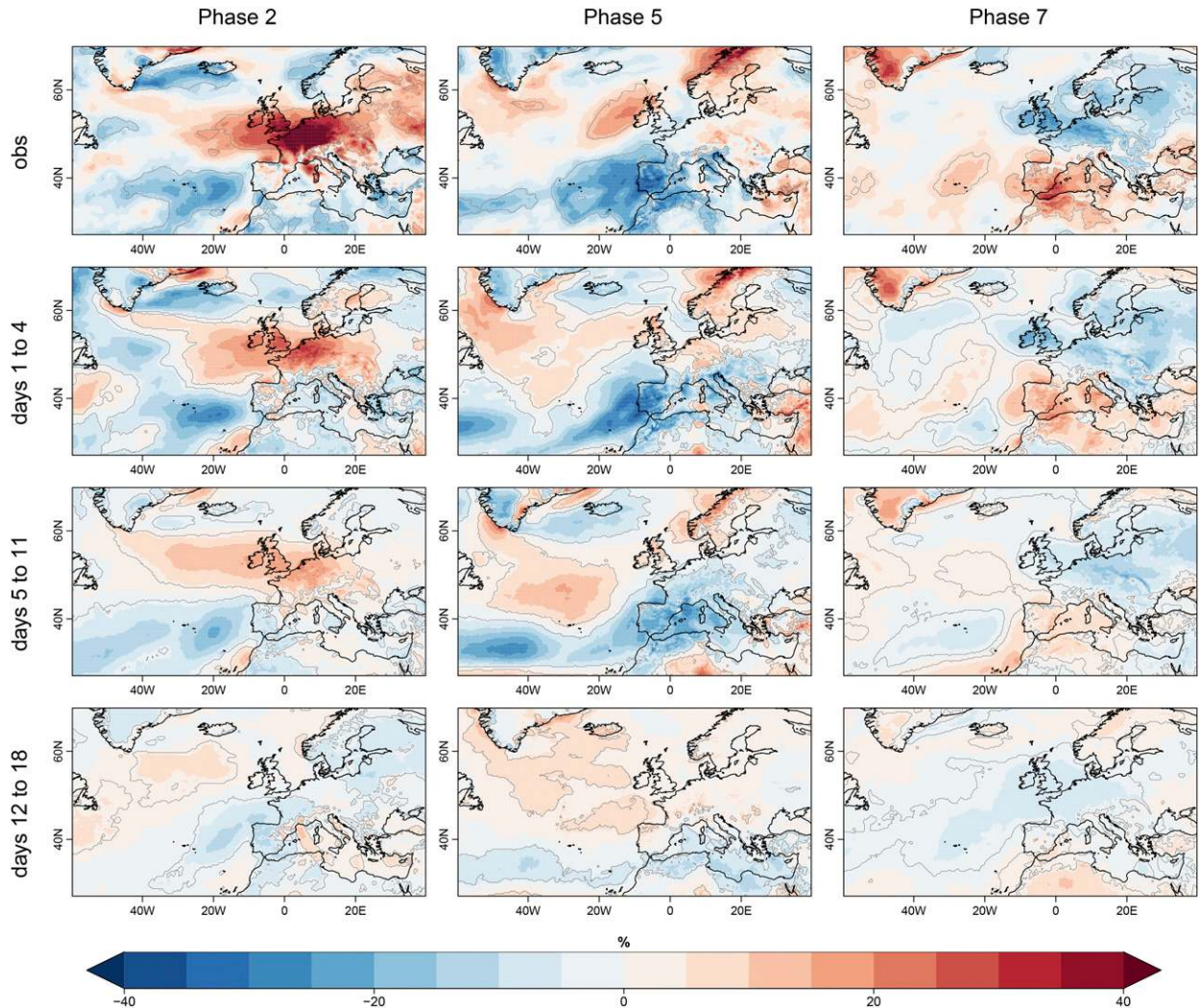
FIG. 5. Surface wind stratifications for phases (left) 2, (center) 5, and (right) 7 from ERA5 and MFS in JFM 1998–2017. (first row) Observed teleconnection impacts as seen in ERA5 (as in last column of Fig. 1). (second to fourth rows) Predicted impacts in MFS for days 1 to 4, 5 to 11 (week 1), and 12 to 18 (week 2), respectively. Gray contours indicate statistical significance at the 95% level.

be done through contingency tables for each of the phases. Instead of that, a more visual verification is proposed here, employing parallel sets plots (Kosara et al. 2006). In Fig. 6 each panel presents the verification for a different range of forecast times. The information of all the contingency tables for each forecast time group can be seen at once in the plot, but the graph also allows to understand phase errors. All the lines that connect one category on the left (forecasts) to the same category on the right (observations) are the hits. All the lines that point toward the Ampl < 2 category are false alarms, while the lines that emerge from Ampl < 2 are misses. Phase errors (lines connecting one strong MJO category to another one) have to be counted also as misses and false alarms, but this graphical separation is more

meaningful than the contingency table. Correct rejections (Ampl < 2 to Ampl < 2) have been omitted in these figures, because they are much more numerous (representing an 83% of the total) and are indeed meaningless to our purposes.

For short forecast times from 1 to 4 days ahead, there are a good amount of hits for all the phases but for phase 4. The number of false alarms is quite small with the misses being especially noticeable for phase 3. When moving to longer forecast times, the number of misses grows substantially, while the false alarms are reduced. By week 1 (days 5 to 11) the number of misses is more than 40% (excluding the correct rejections in the total) and by week 3 (days 19 to 25) the number of hits is reduced to almost nothing. MJO propagation in most
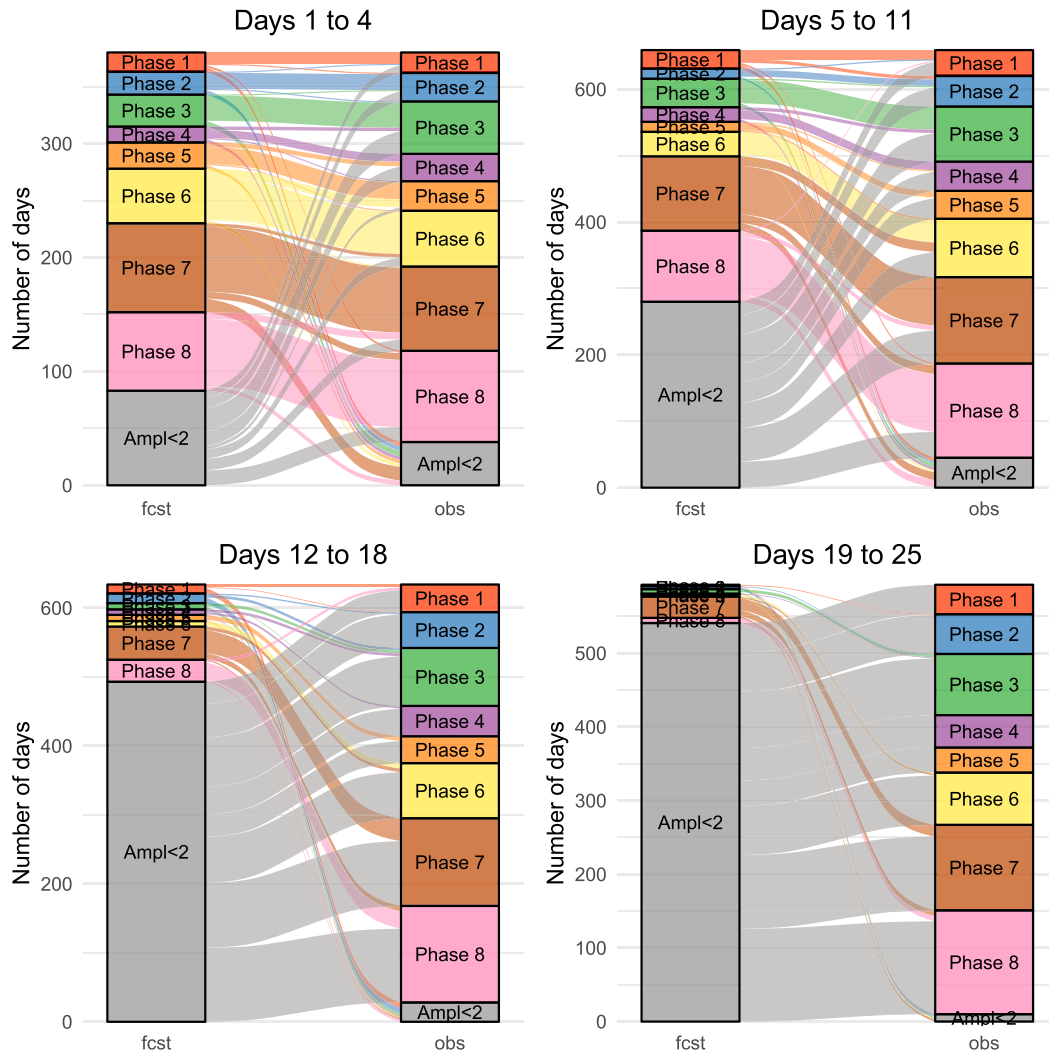
FIG. 6. Verification of ECMWF MFS 2018 categorical forecasts of strong MJO events at four different forecast time ranges: days (top left) 1–4, (top right) 5–11, (bottom left) 12–18, and (bottom right) 19–25. The forecast category is determined from the ensemble-mean S2S MJO forecast, and the observed category is determined from the S2S ERA-Interim-derived MJO index. Each panel employs a parallel sets graph to illustrate correspondence between forecasts on the left side and observations on the right side. The width of the lines is proportional to the number of days in each correspondence relationship. Correct rejections (i.e., lines connecting Ampl < 2 to Ampl < 2) have been omitted for clarity.

subseasonal forecast systems (including MFS) is known to be too slow and to have weaker amplitude than observed (Vitart 2017). These biases can lead to the aforementioned weak skill for strong MJO events. The fact that ensemble-mean fields are being employed to compute MJO forecasts can also affect the amplitudes, as there is some cancellation from individual members before computing the RMM components. However, analyzing the individual ensemble member forecasts does not produce better results (see Fig. S5). In conclusion, although MFS MJO forecasts are skillful in terms of bivariate correlation up to 36 days ahead, the

MFS cannot provide a good categorical forecast of wind speed for strong MJO events unless the MJO forecasts are more realistic in their phase and amplitude.

f. Conditional climatology under perfect knowledge of MJO

The previous section has shown that for lead times of more than 10 days the number of correct forecasts of strong MJO events (i.e., the hits) is low. Therefore, employing these forecasts with the conditional climatology method would produce very marginal benefits only, because the method would be issuing climatology
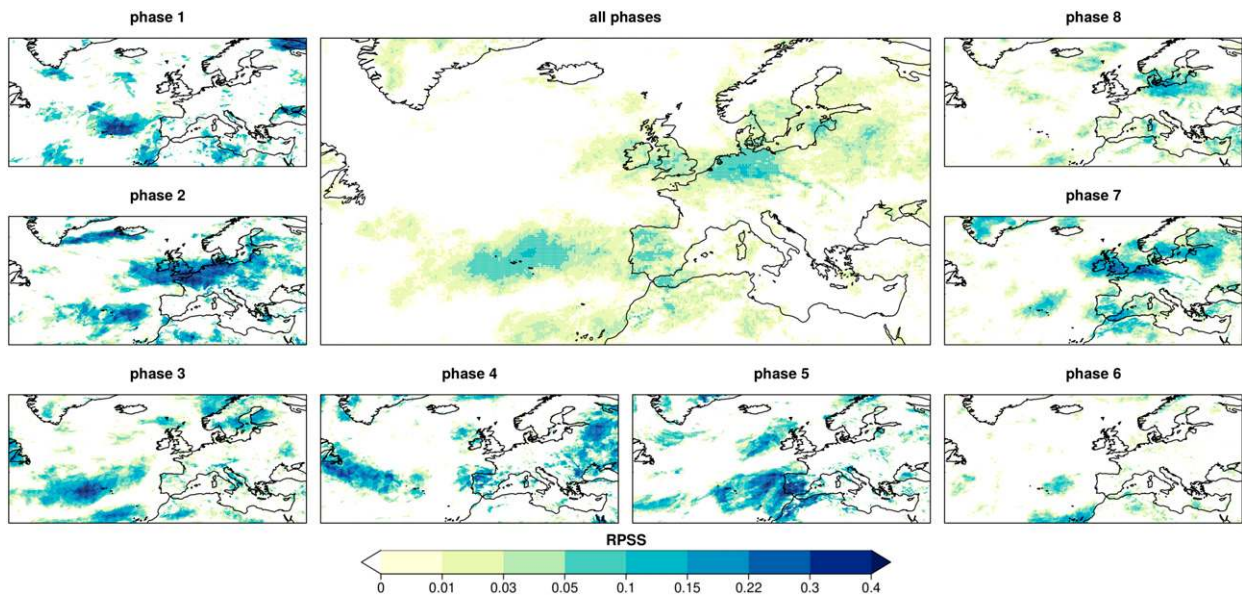
FIG. 7. Ranked probability skill scores of the conditional climatology forecasts under perfect knowledge of the MJO state, (left), (bottom),(right) verified separately for all the days in each MJO phase, and (center) for all the strong MJO events regardless of the MJO phase. Positive values indicate better performance than the benchmark, with 1 representing a perfect forecast.

probabilities for almost all the days. To illustrate the potential that this simple method can bring, it has been used here assuming perfect knowledge of MJO status to produce an upper bound of its skill. MJO forecasts are only made available for the S2S index, therefore for consistency the method is employed with observed terciles conditioned to S2S ERAI-derived MJO index for the 1998–2017 period. The method issues probabilities for tercile categories, and therefore the skill assessment employs the RPSS metric [see section 2b(4)]. Figure 7 shows the RPSS of the conditional climatology predictions for all the days under a strong MJO, and separately for each of the phases. Positive skills (i.e., better performance than climatology) can be seen for all phases in the regions where the observed tercile frequencies differ appreciably from the climatology. The skill reaches values higher than 0.35 over central Europe for phase 2 and 7 or over the Iberian Peninsula for phase 5. When looking at the skill for all days with a strong MJO, values up to 0.1 remain in many parts of Europe, with a pattern that spans the central latitudes of Europe and the Iberian Peninsula. The number of days with a strong MJO (733) is small compared to the whole JFM 1981–2017 sample, representing 22%. Then, when considering the skill for the whole period, the regular climatology dominates the forecasts and the gains that are made during the strong MJO days are diluted (not shown). However, the results show that there is a window of opportunity for employing this method during the days when the MJO is predicted to be in a strong amplitude,

although better MJO forecasts for strong events would be needed for longer forecast times.

4. Conclusions

Deep convection in the tropics is connected to extratropical anomalies of surface wind speed at different time scales through Rossby wave propagation. For instance, convection associated with ENSO or the North Pacific mode influences wind speed in North America at seasonal time scales (Lledó et al. 2018). The MJO associated convection moves eastward at a pace of around 5° of longitude per day, offering an opportunity to analyze its extratropical impacts. An analysis of simultaneous wind speeds over Europe during strong MJO episodes using reanalyses has revealed that large wind anomalies do exist. Their location and strength are a function of the MJO phase, although there are considerable variations among individual events. For instance, recent studies have shown that the MJO teleconnection to Europe can vary substantially with the ENSO phase, which impacts MJO propagation speed (Lee et al. 2019; Wang et al. 2019). The relationship between the phase of strong MJO events and surface wind speed over Europe is a source of predictability that could be employed by the wind energy sector.

Stratifications of wind speed predictions from ECMWF MFS have shown that this subseasonal prediction system is not able to accurately reproduce the expected MJO teleconnection impacts in wind speed over Europe for

lead times of more than 10 days (i.e., whenever a member of the MFS anticipates a strong MJO event more than 10 days ahead the simultaneous wind speed anomalies over Europe do not resemble those observed in the past records). To overcome this limitation, which is also found in other prediction systems (Vitart 2017), a hybrid dynamical–statistical model that combines MJO dynamical forecasts with the observed impacts of the MJO has been proposed. The method employs observed frequencies of above-normal, normal, and below-normal wind speeds during strong MJO events as probabilistic forecasts whenever a strong MJO event is anticipated. This method—named conditional climatology—has been tested under perfect knowledge of the MJO state, showing that it has the potential to deliver categorical probabilistic predictions of daily mean wind speed that are better than the reference climatology in many European regions. However, although MFS can skillfully predict the MJO evolution up to 36 days ahead in terms of bivariate correlation, strong MJO events cannot be skillfully predicted more than 10 days ahead. The inability to anticipate strong MJO events poses a barrier to the effective application of this method.

In summary this research has shown that 1) strong MJO events have an effect on surface winds in Europe; 2) analyzing the most frequently observed terciles under each MJO phase provides a more robust analysis of the diversity of MJO impacts; 3) the BoM and S2S MJO indices produce significant differences in terms of strong MJO events; 4) the MFS cannot anticipate strong MJO events more than 10 days ahead; and 5) an hybrid statistical–dynamical method could deliver good performance levels weeks ahead if better predictions for strong MJO events were available. Overall, this research highlights the relevance of tropical–extratropical interactions for enhancing subseasonal predictions in the extratropics, and for anticipating surface conditions that impact climate-vulnerable sectors weeks ahead. This paper illustrates that the MJO plays a limited role in defining the daily wind speed in Europe, even if its features were much better predicted by future subseasonal forecast systems. Hence, the usefulness of subseasonal predictions for sectors vulnerable to surface wind variability requires paying attention to the multiple factors that determine the atmospheric circulation in the area at those time scales.

REFERENCES

Adames, Á. F., and J. M. Wallace, 2014: Three-dimensional structure and evolution of the MJO and its relation to the mean flow. *J. Atmos. Sci.*, **71**, 2007–2026, https://doi.org/10.1175/JAS-D-13-0254.1.

Barnes, E. A., S. M. Samarasinghe, I. Ebert-Uphoff, and J. C. Furtado, 2019: Tropospheric and stratospheric causal pathways between the MJO and NAO. *J. Geophys. Res. Atmos.*, **124**, 9356–9371, https://doi.org/10.1029/2019jd031024.

Cassou, C., 2008: Intraseasonal interaction between the Madden–Julian Oscillation and the North Atlantic oscillation. *Nature*, **455**, 523–527, https://doi.org/10.1038/nature07286.

Copernicus Climate Change Service (C3S), 2017: ERA5: Fifth generation of ECMWF atmospheric reanalyses of the global climate. Copernicus Climate Change Service Climate Data Store (CDS), accessed 1 June 2019, https://cds.climate.copernicus.eu/cdsapp#!/home.

Dee, D. P., and Coauthors, 2011: The ERA-Interim reanalysis: Configuration and performance of the data assimilation system. *Quart. J. Roy. Meteor. Soc.*, **137**, 553–597, https://doi.org/10.1002/qj.828.

ECMWF, 2019: The ECMWF monthly forecasting system. ECMWF, accessed 15 May 2019, https://www.ecmwf.int/en/forecasts/documentation-and-support/extended-range-forecasts/ecmwf-monthly-forecasting-system.

Gelaro, R., and Coauthors, 2017: The Modern-Era Retrospective Analysis for Research and Applications, version 2 (MERRA-2). *J. Climate*, **30**, 5419–5454, https://doi.org/10.1175/JCLI-D-16-0758.1.

Gottschalck, J., and Coauthors, 2010: A framework for assessing operational Madden–Julian Oscillation forecasts. *Bull. Amer. Meteor. Soc.*, **91**, 1247–1258, https://doi.org/10.1175/2010BAMS2816.1.

Jolliffe, I. T., and D. B. Stephenson, Eds., 2012: *Forecast Verification: A Practitioner's Guide in Atmospheric Science.* 2nd ed. John Wiley & Sons, 274 pp., https://doi.org/10.1002/9781119960003.

Jupp, T. E., R. Lowe, C. A. S. Coelho, and D. B. Stephenson, 2012: On the visualization, verification and recalibration of ternary probabilistic forecasts. *Philos. Trans. Roy. Soc.*, **A370**, 1100–1120, https://doi.org/10.1098/rsta.2011.0350.

Kalnay, E., and Coauthors, 1996: The NCEP/NCAR 40-Year Reanalysis Project. *Bull. Amer. Meteor. Soc.*, **77**, 437–471, https://doi.org/10.1175/1520-0477(1996)077<0437:TNYRP>2.0.CO;2.

Kim, H., M. A. Janiga, and K. Pegion, 2019: MJO propagation processes and mean biases in the SubX and S2S reforecasts. *J. Geophys. Res. Atmos.*, **124**, 9314–9331, https://doi.org/10.1029/2019jd031139.

Kosara, R., F. Bendix, and H. Hauser, 2006: Parallel sets: Interactive exploration and visual analysis of categorical data. *IEEE Trans. Vis. Comput. Graph.*, **12**, 558–568, https://doi.org/10.1109/TVCG.2006.76.

Lee, R. W., S. J. Woolnough, A. J. Charlton-Perez, and F. Vitart, 2019: ENSO modulation of MJO teleconnections to the north Atlantic and Europe. *Geophys. Res. Lett.*, **46**, 13 535–13 545, https://doi.org/10.1029/2019GL084683.

Lim, Y., S.-W. Son, and D. Kim, 2018: MJO prediction skill of the subseasonal-to-seasonal prediction models. *J. Climate*, **31**, 4075–4094, https://doi.org/10.1175/JCLI-D-17-0545.1.

——, ——, A. G. Marshall, H. H. Hendon, and K.-H. Seo, 2019: Influence of the QBO on MJO prediction skill in the subseasonal-to-seasonal prediction models. *Climate Dyn.*, **53**, 1681–1695, https://doi.org/10.1007/s00382-019-04719-y.

Lin, H., G. Brunet, and J. Derome, 2008: Forecast skill of the Madden–Julian Oscillation in two Canadian atmospheric models. *Mon. Wea. Rev.*, **136**, 4130–4149, https://doi.org/10.1175/2008MWR2459.1.

——, ——, and ——, 2009: An observed connection between the North Atlantic Oscillation and the Madden–Julian oscillation. *J. Climate*, **22**, 364–380, https://doi.org/10.1175/2008JCLI2515.1.

Liu, P., Q. Zhang, C. Zhang, Y. Zhu, M. Khairoutdinov, H.-M. Kim, C. Schumacher, and M. Zhang, 2016: A revised real-time multivariate MJO index. *Mon. Wea. Rev.*, **144**, 627–642, https://doi.org/10.1175/MWR-D-15-0237.1.

Lledó, L., O. Bellprat, F. J. Doblas-Reyes, and A. Soret, 2018: Investigating the effects of Pacific sea surface temperatures on the wind drought of 2015 over the United States. *J. Geophys. Res. Atmos.*, **123**, 4837–4849, https://doi.org/10.1029/2017JD028019.

Madden, R. A., and P. R. Julian, 1971: Detection of a 40–50 day oscillation in the zonal wind in the tropical Pacific. *J. Atmos. Sci.*, **28**, 702–708, https://doi.org/10.1175/1520-0469(1971)028<0702:DOADOI>2.0.CO;2.

——, and ——, 1972: Description of global-scale circulation cells in the tropics with a 40–50 day period. *J. Atmos. Sci.*, **29**, 1109–1123, https://doi.org/10.1175/1520-0469(1972)029<1109:DOGSCC>2.0.CO;2.

Ramon, J., L. Lledó, V. Torralba, A. Soret, and F. J. Doblas-Reyes, 2019: What global reanalysis best represents near-surface winds? *Quart. J. Roy. Meteor. Soc.*, **145**, 3236–3251, https://doi.org/10.1002/qj.3616.

Rashid, H. A., H. H. Hendon, M. C. Wheeler, and O. Alves, 2010: Prediction of the Madden–Julian Oscillation with the POAMA dynamical prediction system. *Climate Dyn.*, **36**, 649–661, https://doi.org/10.1007/s00382-010-0754-x.

Soret, A., and Coauthors, 2019: Sub-seasonal to seasonal climate predictions for wind energy forecasting. *J. Phys. Conf. Ser.*, **1222**, 012009, https://doi.org/10.1088/1742-6596/1222/1/012009.

Straub, K. H., 2013: MJO initiation in the real-time multivariate MJO index. *J. Climate*, **26**, 1130–1151, https://doi.org/10.1175/JCLI-D-12-00074.1.

Torralba, V., 2019: Seasonal climate prediction for the wind energy sector: Methods and tools for the development of a climate service. Ph.D. thesis, Universidad Complutense de Madrid, 296 pp.

——, F. J. Doblas-Reyes, I. Jiménez, L. Lledó, N. González-Reviriego, and A. Soret, 2016: Development of a wind energy climate service based on seasonal climate prediction. *Third BSC Int. Doctoral Symp.*, Barcelona, Spain, Barcelona Supercomputing Center, 43–45, https://doi.org/10.13140/rg.2.2.18352.15362.

Vitart, F., 2004: Monthly forecasting at ECMWF. *Mon. Wea. Rev.*, **132**, 2761–2779, https://doi.org/10.1175/MWR2826.1.

——, 2017: Madden–Julian Oscillation prediction and teleconnections in the S2S database. *Quart. J. Roy. Meteor. Soc.*, **143**, 2210–2220, https://doi.org/10.1002/qj.3079.

——, and Coauthors, 2017: The Subseasonal to Seasonal (S2S) prediction project database. *Bull. Amer. Meteor. Soc.*, **98**, 163–173, https://doi.org/10.1175/BAMS-D-16-0017.1.

Wang, B., G. Chen, and F. Liu, 2019: Diversity of the Madden–Julian Oscillation. *Sci. Adv.*, **5**, eaax0220, https://doi.org/10.1126/sciadv.aax0220.

Wheeler, M. C., and H. H. Hendon, 2004: An all-season real-time multivariate MJO index: Development of an index for monitoring and prediction. *Mon. Wea. Rev.*, **132**, 1917–1932, https://doi.org/10.1175/1520-0493(2004)132<1917:AARMMI>2.0.CO;2.

Wilks, D. S., Ed., 2011: Statistical forecasting. *Statistical Methods in the Atmospheric Sciences*, Academic Press, 215–300.

Zhang, C., 2005: Madden–Julian Oscillation. *Rev. Geophys.*, **43**, RG2003, https://doi.org/10.1029/2004RG000158.

——, 2013: Madden–Julian Oscillation: Bridging weather and climate. *Bull. Amer. Meteor. Soc.*, **94**, 1849–1870, https://doi.org/10.1175/BAMS-D-12-00026.1.

——, and B. Zhang, 2018: QBO–MJO connection. *J. Geophys. Res. Atmos.*, **123**, 2957–2967, https://doi.org/10.1002/2017JD028171.

Zheng, C., and E. K. M. Chang, 2019: The role of MJO propagation, lifetime, and intensity on modulating the temporal evolution of the MJO extratropical response. *J. Geophys. Res. Atmos.*, **124**, 5352–5378, https://doi.org/10.1029/2019JD030258.